

# Estimating black carbon aging time-scales with a particle-resolved aerosol model

Nicole Riemer <sup>a,\*</sup>, Matthew West <sup>b</sup>, Rahul Zaveri <sup>c</sup>,  
Richard Easter <sup>c</sup>

<sup>a</sup>*Department of Atmospheric Science, University of Illinois at Urbana-Champaign,  
Urbana, Illinois, USA*

<sup>b</sup>*Department of Mechanical Science and Engineering, University of Illinois at  
Urbana-Champaign, Urbana, Illinois, USA*

<sup>c</sup>*Atmospheric Science and Global Change Division, Pacific Northwest National  
Laboratory, Richland, Washington, USA*

---

## Abstract

Understanding the aging process of aerosol particles is important for assessing their chemical reactivity, cloud condensation nuclei activity, radiative properties and health impacts. In this study we investigate the aging of black carbon containing particles in an idealized urban plume using a new approach, the particle-resolved aerosol model PartMC-MOSAIC. We present a method to estimate aging time-scales using an aging criterion based on cloud condensation nuclei activation. The results show a separation into a daytime regime where condensation dominates and a nighttime regime where coagulation dominates. For the chosen urban plume scenario, depending on the supersaturation threshold, the values for the aging time-scales vary between 0.06 hours and 10 hours during the day, and between 6 hours and 20 hours during the night.

*Key words:* black carbon, aerosol aging, mixing state, CCN

---

## 1 Introduction

Black carbon containing particles, or “soot” particles, are ubiquitous in the atmosphere and their role for regional and global climate has been widely recognized (IPCC, 2007). Since black carbon absorbs light (Horvath and Trier,

---

\* Corresponding author

*Email address:* `nriemer@illinois.edu` (Nicole Riemer).

1993), it contributes to the aerosol radiative forcing, potentially partially offsetting the cooling effect of scattering aerosol particles such as sulfates (Menon et al., 2002).

Black carbon containing particles originate from the incomplete combustion of carbon containing material, hence emissions from traffic are an important contributor (Bond et al., 2004). Other important sources for black carbon include biomass burning and the combustion of coal by industrial processes. In this paper we focus on black carbon from traffic emissions. Measurements of vehicle emissions from gasoline and diesel cars show that the emitted particles are a complex mixture of many chemical species with the main constituents being black carbon and organic carbon (Medalia and Rivin, 1982; Toner et al., 2006). Trace concentrations of ionic and metallic species are also present (Kleeman et al., 2000). The exact composition depends on several factors, including the fuel type, the operating conditions and the condition of the individual vehicles.

During their transport in the atmosphere, the composition of these particle emissions are further modified. Coagulation, condensation and photochemistry are contributing processes, collectively known as aging (Weingartner et al., 1997). During this aging process the composition of the individual particles or, in other words, their mixing states change (Furutani et al., 2008). This impacts the particles' physico-chemical properties including their chemical reactivity, radiative properties and health impacts. In particular, the aging process can change the particles' hygroscopicity from initially hydrophobic to more hydrophilic, and hence change their ability to become cloud condensation nuclei (McFiggans et al., 2006; McMurry and Stolzenburg, 1989; Moffet et al., 2008; Cubison et al., 2008).

This is important as models and observations suggest that wet deposition represents 70–85% of the tropospheric sink for carbonaceous aerosol mass (Pöschl, 2005). As a consequence, to assess the budget and impact of black carbon, models need to capture the aging process adequately. Many global models have simulated both (fresh) hydrophobic black carbon and (aged) hydrophilic black carbon, which can be considered a minimal representation of the black carbon mixing state (Cooke et al., 1999; Lohmann et al., 1999; Koch, 2001; Croft et al., 2005). In such a framework only the hydrophilic black carbon is subject to in-cloud scavenging. The conversion from hydrophobic to hydrophilic is frequently modeled as a first-order system with the single parameter of aging rate or its inverse, the aging time-scale  $\tau$  which represents the time-scale on which a population of black carbon containing particles transfers from the “fresh” category to the “aged” category.

While conceptually simple, the actual value of the aging time-scale  $\tau$  is not well constrained. Koch (2001) and Croft et al. (2005) compared different aging parameterizations in global models and concluded that the model results

critically depended on the respective formulation. Riemer et al. (2004) used mesoscale simulations to determine  $\tau$ . They derived the aging time-scale for black carbon particles as a function of height and time of the day, which suggested that assuming a single parameter for the black carbon aging time-scale is an oversimplification that will incorrectly estimate the black carbon burden. However, even though this treatment allowed more detailed insight into the aging process, it was still based on ad hoc aging rules inherent to the modal model framework that was used (Riemer et al., 2003).

Recently, Riemer et al. (2009) developed a particle-resolved aerosol model, PartMC-MOSAIC, which explicitly resolves the composition of individual particles in a given population of different types of aerosol particles, so that no ad hoc aging criteria needs to be invoked. They applied PartMC-MOSAIC in a Lagrangian box-model framework to an idealized urban plume scenario to study the evolution of urban aerosols due to coagulation and condensation over the course of 24 hours.

In this study, we build upon Riemer et al. (2009) and present a method for estimating aging time-scales of black carbon containing particles using PartMC-MOSAIC, based on the idealized urban plume scenario. We take the particle population simulated in Riemer et al. (2009) and use a CCN-based aging criteria to determine whether each individual particle is fresh or aged at every timestep, and how many particles transfer between the fresh and aged categories during each timestep. By fitting these results to a first-order bulk model of aerosol aging we are able to determine the aging timescale without making any a priori assumptions about the aging process. To our knowledge it is the first time that a method is presented for explicitly calculating aging time-scales.

Section 2 introduces the model system. In Section 3 we describe the idealized plume scenario that served as a basis for the time-scale estimation. Section 4 presents our method for deriving time-scales from our model and Section 5 shows the results. We summarize our findings in Section 6.

## 2 Model description

PartMC-MOSAIC is a particle-resolved model that simulates the evolution of individual aerosol particles and trace gases in a single parcel (or volume) of air moving along a specified trajectory. For each particle the mass of each constituent species is tracked, but the particle position in space is not simulated, making this a zero-dimensional or box model. In addition to coagulation and aerosol- and gas-phase chemistry, the model includes prescribed emissions of aerosols and gases, and mixing of the parcel with background air. The simu-

84 lation results shown here use around 100,000 particles in a volume of around  
85  $16\text{ cm}^3$  (the precise values vary over the course of the simulation). We regard  
86 this volume as being representative of a much larger air parcel. The model  
87 accurately predicts both number and mass size distributions and is therefore  
88 suited for applications where either quantity is required. Details of PartMC-  
89 MOSAIC and the urban plume scenario are described in Riemer et al. (2009).  
90 Here we give a brief summary.

91 The simulation of the aerosol state proceeds by two mechanisms. First, the  
92 composition of each particle can change as species condense from the gas phase  
93 and evaporate to it. Second, the aerosol population can have particles added  
94 and removed, either by coagulation events between particles, by emissions,  
95 or by dilution. While condensation/evaporation is handled deterministically,  
96 emission, dilution and coagulation are treated with a stochastic approach.

97 Coagulation between aerosol particles is simulated in PartMC by generating  
98 a realization of a Poisson process with a Brownian coagulation kernel. For  
99 the large number of particles used here it is necessary to employ an efficient  
100 approximate simulation method. We developed a binned sampling method  
101 to efficiently sample from the highly multi-scale coagulation kernel (in our  
102 case the Brownian kernel) in the presence of a very non-uniform particle size  
103 distribution, which is described in detail in Riemer et al. (2009).

104 Particle emissions and dilution with background air are also implemented  
105 in a stochastic manner. Because we are using a finite number of particles to  
106 approximate the current aerosol population, we need to add a finite number of  
107 emitted particles to the volume at each timestep. Over time these finite particle  
108 samplings should approximate the continuum emission distribution, so the  
109 samplings at each timestep must be different. As for coagulation, we assume  
110 that emissions are memoryless, so that emission of each particle is uncorrelated  
111 with emission of any other particle. Under this assumption the appropriate  
112 statistics are Poisson distributed, whereby the distribution of finite particles  
113 is parametrized by the mean emission rate and distribution.

114 Lastly, we must also obtain a finite sampling of background particles that have  
115 diluted into our computational volume during each timestep. In addition, some  
116 of the particles in our current sample will dilute out of our volume and will  
117 be lost, so this must be sampled as well. Again, we assume that dilution is  
118 memoryless, so that dilution of each particle is uncorrelated with the dilution  
119 of any other particle or itself at other times, and that once a particle dilutes  
120 out it is lost.

121 We coupled the stochastic PartMC particle-resolved aerosol model to the de-  
122 terministic MOSAIC gas- and aerosol-chemistry code (Zaveri et al., 2008)  
123 in a time- or operator-splitting fashion (Press et al., 2007, Section 20.3.3).

124 MOSAIC treats all the globally important aerosol species including sulfate,  
125 nitrate, chloride, carbonate, ammonium, sodium, calcium, primary organic  
126 aerosol (POA), secondary organic aerosol (SOA), black carbon (BC), and in-  
127 ert inorganic mass.

128 MOSAIC consists of four computationally efficient modules: 1) the gas-phase  
129 photochemical mechanism CBM-Z (Zaveri and Peters, 1999); 2) the Multicom-  
130 ponent Taylor Expansion Method (MTEM) for estimating activity coefficients  
131 of electrolytes and ions in aqueous solutions (Zaveri et al., 2005b); 3) the Mul-  
132 ticomponent Equilibrium Solver for Aerosols (MESA) for intra-particle solid-  
133 liquid partitioning (Zaveri et al., 2005a); and 4) the Adaptive Step Time-split  
134 Euler Method (ASTEM) for dynamic gas-particle partitioning over size- and  
135 composition-resolved aerosol (Zaveri et al., 2008). The version of MOSAIC  
136 implemented here also includes a treatment for SOA based on the SORGAM  
137 scheme (Schell et al., 2001).

### 138 3 Idealized urban plume scenario

139 For our urban plume scenario, we tracked the evolution of gas phase species  
140 and aerosol particles in a Lagrangian air parcel that initially contained back-  
141 ground air and was advected over and beyond a large urban area, as described  
142 in Riemer et al. (2009). The simulation started at 06:00 local standard time  
143 (LST), and during the advection process, primary trace gases and aerosol par-  
144 ticles from different sources were emitted into the air parcel for the duration  
145 of 12 hours. After 18:00 LST, all emissions were switched off, and the evo-  
146 lution of the air parcel was tracked for another 12 hours. The time series of  
147 temperature, relative humidity and mixing height are shown in Figure 1.

148 Initial gas-phase and aerosol particle concentrations as well as gas phase and  
149 particle emissions were the same as in Riemer et al. (2009). The gas phase  
150 emissions varied throughout the emission time interval according to a typical  
151 diurnal cycle found in polluted urban areas.

152 The initial particle distribution, which was identical to the background aerosol  
153 distribution, was bimodal with Aitken and accumulation modes (Jaenicke,  
154 1993). We assumed that it consisted of  $(\text{NH}_4)_2\text{SO}_4$  and POA, as shown in Ta-  
155 ble 1. We considered three different types of carbonaceous aerosol emissions:  
156 1) meat cooking aerosol, 2) diesel vehicle emissions, and 3) gasoline vehicle  
157 emissions. The parameters for the distributions of these three emission cate-  
158 gories were based on Eldering and Cass (1996), Kittelson et al. (2006a), and  
159 Kittelson et al. (2006b), respectively. For simplicity in this idealized study, the  
160 particle emissions strength and their size distribution and composition were  
161 kept constant with time during the time period of emission.

162 Furthermore, we assumed that every particle from a given source had the  
 163 same composition, with the species listed in Table 1, since to date the mixing  
 164 state of particle emissions is still not well quantified. In particular, we assume  
 165 that the diesel and gasoline exhaust particles consist exclusively of POA and  
 166 BC, which is very nearly the case (Andreae and Gelenc  ser, 2006; Medalia and  
 167 Rivin, 1982; Kleeman et al., 2000).

168 Figure 2 shows time series of the bulk aerosol mass concentrations as they  
 169 result from this urban plume scenario. We observed a pronounced production  
 170 of ammonium nitrate, reaching nitrate mass concentration of up to  $26 \mu\text{g m}^{-3}$   
 171 and ammonium mass concentration of  $10 \mu\text{g m}^{-3}$  in the late afternoon. Sulfate  
 172 mass concentrations increased from  $4.1 \mu\text{g m}^{-3}$  to  $6.0 \mu\text{g m}^{-3}$  due to conden-  
 173 sation of photochemically produced sulfuric acid. POA and BC were directly  
 174 emitted (with a temporally constant rate) and accumulated to  $11 \mu\text{g m}^{-3}$  and  
 175  $4.3 \mu\text{g m}^{-3}$ , respectively, until 18:00 LST when the emissions stopped. After  
 176 18:00 LST the mass concentrations declined due to dilution, especially nitrate  
 177 and BC for which the background mass concentration were zero.

### 178 3.1 Characterizing mixing state

To characterize the mixing state and to discuss the composition of a particle,  
 we refer to the BC mass fractions as

$$w_{\text{BC,dry}} = \frac{\mu_{\text{BC}}}{\mu_{\text{dry}}} \quad (1)$$

179 where  $\mu_{\text{BC}}$  is the mass of BC in a given particle and  $\mu_{\text{dry}}$  is the total dry mass.

180 Based on this quantity, we then define a two-dimensional number concen-  
 181 tration that is a function of both particle composition and diameter. The  
 182 two-dimensional cumulative number distribution  $N_{\text{BC,dry}}(w, D)$  is the number  
 183 of particles per volume that have a diameter less than  $D$  and a BC mass  
 184 fraction of less than  $w$ . The top panels in Figure 3 show the corresponding  
 185 two-dimensional distributions, normalized with the respective total number  
 186 concentrations, after 1 hour and after 24 hours of simulation time. Since even  
 187 at the time of emission no particles were pure BC, particles were not present  
 188 at  $w_{\text{BC,dry}} = 100\%$ . Fresh emissions from diesel vehicles ( $w_{\text{BC,dry}} = 70\%$ ) and  
 189 gasoline vehicles ( $w_{\text{BC,dry}} = 20\%$ ) appear as horizontal lines since particles  
 190 in one emission category were all emitted with the same composition. At  
 191  $w_{\text{BC,dry}} = 0\%$  all the particles appear that do not contain any BC (i.e. back-  
 192 ground particles and particles from meat cooking emissions that have not un-  
 193 dergone coagulation with particles containing BC). After 1 hour (07:00 LST)  
 194 a small number of particles between these three classes indicate the occur-  
 195 rence of coagulation. Comparing this result to the result for the end of the

simulation, we note that at the end of the simulation particles with diameter below  $D = 0.03 \mu\text{m}$  were heavily depleted due to coagulation. A continuum of mixing states formed between the extreme mixing states of  $w_{\text{BC,dry}} = 0\%$  and  $w_{\text{BC,dry}} = 70\%$ .

### 3.2 Calculating CCN activity

Given that we track the composition evolution of each individual particle throughout the simulation, we can calculate the critical supersaturation  $S_c$  that the particle needs in order to activate. We use the concept of a dimensionless hygroscopicity parameter suggested by Ghan et al. (2001) or Petters and Kreidenweis (2007). In Petters and Kreidenweis (2007) this parameter is denoted by  $\kappa$ , and we adopt their notation for the remainder of the paper. This concept has the advantage that results from laboratory measurements can be used to quantify the hygroscopicity of complex compounds for which  $\kappa$  values cannot be calculated in a straightforward manner. The overall  $\kappa$  for a particle is the volume-weighted average of the  $\kappa$  values of the constituent species. This requires the assignment of individual  $\kappa$  values for each aerosol component in MOSAIC.

Petters and Kreidenweis (2007) compiled a table (Table 1 in their paper) with  $\kappa$  values for a variety of inorganic and organic species based on recent laboratory measurements or on thermodynamic model calculations. For  $(\text{NH}_4)_2\text{SO}_4$  and  $\text{NH}_4\text{NO}_3$  they report  $\kappa$  values of 0.61 and 0.67, based on calculations by Clegg et al. (1998) and measurements by Svenningsson et al. (2006), respectively. Based on this we assume  $\kappa = 0.65$  for all salts formed from the  $\text{NH}_4^+ - \text{SO}_4^{2-} - \text{NO}_3^-$  system. For all MOSAIC model species that represent SOA we assume  $\kappa = 0.1$ , based on measurements by Prenni et al. (2007). Following Petters et al. (2006) we assume  $\kappa = 0.001$  for POA and  $\kappa = 0$  for BC. The critical supersaturation  $S_c$  for a particle of diameter  $D$  and volume-weighted hygroscopicity parameter  $\kappa$  is then given by

$$S_c = \frac{C}{\sqrt{\kappa D^3}}, \quad (2)$$

where

$$C = \sqrt{\frac{4A^3}{27}} \quad \text{and} \quad A = \frac{4\sigma_w m_w}{R^* T \rho_w}, \quad (3)$$

with  $\sigma_w$  being the surface tension of water,  $m_w$  the molecular weight of water,  $R^*$  the universal gas constant,  $\rho_w$  the water density, and  $T$  the temperature.

Similarly to the use of  $w_{\text{BC,dry}}$  above, we can use  $S_c$  to define a two-dimensional cumulative number distribution  $N_S(D, S_c)$  in terms of size and critical supersaturation. The bottom panels in Figure 3 show examples of the corresponding

218 two-dimensional distributions after 1 hour (left) and after 24 hours (right) of  
 219 simulation. While freshly emitted diesel, gasoline and meat cooking particles  
 220 differ in their BC and POA mass fractions, they are very similar in their hy-  
 221 groscopicity with initial  $\kappa$  values close to zero. After 1 hour they are visible  
 222 as the dark band of high number concentrations at high  $S_c$  values. Separated  
 223 from this we see another dark band representing the most hygroscopic parti-  
 224 cles, consisting of wet background particles. They contain the largest fraction  
 225 of inorganic mass (ammonium, sulfate, and nitrate), hence their critical su-  
 226 persaturation is lowest at a given size compared to the other particle classes.

227 Directly slightly above the most hygroscopic band at 1 hour is a weaker band,  
 228 which represents the dry background particles. Because they are dry and the  
 229 vapor pressure of  $\text{HNO}_3$  is still low, nitrate formation does not occur on these  
 230 particles. The coexistence of wet and dry particles can be explained by the  
 231 fact that the relative humidity falls below 85% at 06:42 LST, which is the del-  
 232 liquescence point of the inorganic mixture of ammonium, sulfate, and nitrate.  
 233 Particles that exist before that time contain water and take up nitrate. They  
 234 stay wet throughout the whole day as a result of the hysteresis of particle  
 235 deliquescence and crystallization. Particles that are emitted after 06:42 LST  
 236 do not contain water and take up nitrate only much later. Hence after 1 hour  
 237 of simulation, at a given size the fraction of highly hygroscopic inorganics is  
 238 higher for the wet particles, which results in a higher  $\kappa$  value and lower critical  
 239 supersaturation  $S_c$ .

240 The individual bands are not completely separated at 1 hour, but the regions  
 241 in between have started to fill out. The reason for this is the occurrence of  
 242 coagulation, which produces particles of intermediate composition and hence  
 243 corresponding intermediate  $S_c$  values. After 24 hours the population as a whole  
 244 has moved to lower critical supersaturations, and the distribution with respect  
 245 to  $S_c$  has become more continuous. Given a certain size, the critical supersat-  
 246 uration ranges over about one order of magnitude.

247 Figure 4 shows CCN properties as more traditional CCN spectra. This repre-  
 248 sentation is the one-dimensional projection of the bottom panels of Figure 3  
 249 onto the critical supersaturation axis, plotted as a cumulative distribution.  
 250 The change in CCN properties over the course of 24 hours is obvious. After  
 251 1 hour a supersaturation of  $S = 1.5\%$  is necessary to activate 50% of the  
 252 particles by number. This required supersaturation decreases to  $S = 0.1\%$   
 253 after 24 hours. In the following section we use the results of this urban plume  
 254 scenario as a basis for estimating the aging time-scales.

## 255 4 First-order Models of Aging

256 In this section we describe the first-order model of black carbon aging to which  
 257 we fit the particle-resolved data simulated with PartMC-MOSAIC, in order  
 258 to determine the aging time-scale. We emphasize that we do not actually  
 259 simulate using the first-order models presented in this section. Such first-  
 260 order systems are frequently used, however, to model the conversion from  
 261 hydrophobic to hydrophilic black carbon with the single parameter of aging  
 262 rate or its inverse, the aging time-scale  $\tau$  (Croft et al., 2005). More specifically,  
 263 the aging time-scale represents the time-scale on which particles that would  
 264 initially not activate turn into particles that can be activated, given a certain  
 265 chosen supersaturation threshold. Budget equations for the fresh and aged  
 266 populations can be formulated in terms of either number or mass. A number  
 267 based aging time-scale is relevant for aerosol indirect forcing as the cloud  
 268 optical properties depend on the cloud droplet number distribution. On the  
 269 other hand, a mass aging time-scale is relevant for in-cloud scavenging and wet  
 270 removal of BC mass. In the following we will present results for both number-  
 271 and mass-based aging time-scales.

272 At time  $t$ , the total number concentration  $N_{\text{BC}}(t)$  of BC-particles is the sum  
 273 of the number concentration of BC-containing fresh particles  $N_{\text{f}}(t)$  and the  
 274 number concentration of BC-containing aged particles  $N_{\text{a}}(t)$ . We define anal-  
 275 ogously the total BC mass concentration  $M_{\text{BC}}(t)$ , the BC mass concentration  
 276 in fresh BC-containing particles  $M_{\text{f}}(t)$ , and the BC mass concentration in aged  
 277 BC-containing particles  $M_{\text{a}}(t)$ . The aged and fresh populations are separated  
 278 by applying an aging criterion, in our case activation at a certain supersat-  
 279 uration threshold  $S_{\text{c}}$ . Fresh particles are those with critical supersaturation  
 280 above the threshold value, while aged particles have critical supersaturations  
 281 below the threshold.

In the PartMC model we explicitly track a finite number of particles in a com-  
 putational volume  $V$ . The number of fresh and aged BC-containing particles  
 in the volume  $V(t_k)$  at time  $t_k$  is denoted by  $n_{\text{f}}(t_k)$  and  $n_{\text{a}}(t_k)$ , respectively.  
 Similarly,  $m_{\text{f}}(t_k)$  and  $m_{\text{a}}(t_k)$  are respectively the total mass of BC in fresh and  
 aged BC-containing particles in  $V(t_k)$ . The number and mass concentrations  
 of fresh BC-containing particles in  $V(t_k)$  are then given by

$$\begin{aligned} N_{\text{f}}(t_k) &= \frac{n_{\text{f}}(t_k)}{V(t_k)} & M_{\text{f}}(t_k) &= \frac{m_{\text{f}}(t_k)}{V(t_k)} \\ N_{\text{a}}(t_k) &= \frac{n_{\text{a}}(t_k)}{V(t_k)} & M_{\text{a}}(t_k) &= \frac{m_{\text{a}}(t_k)}{V(t_k)}. \end{aligned} \quad (4)$$

282 The fresh and aged number and mass concentrations can change due to emis-  
 283 sion and dilution, while condensation and coagulation can transfer number

284 and mass concentration from the fresh to the aged population and vice versa.  
 285 Changes in number and mass concentrations also occur due to temperature  
 286 and pressure changes. In our model we neglect at present the impact of hetero-  
 287 geneous reactions on the surface of the particles, although studies have shown  
 288 that these also contribute to the aging process (Rudich et al., 2007). The gain  
 289 and loss terms for the fresh and aged BC-containing populations are given in  
 290 Table 2.

291 To express changes in number and mass for coagulation we consider that all  
 292 constituent particles are lost during a coagulation event and the product of  
 293 coagulation is a gain of a new particle. Table 3 shows the overview of all  
 294 possible combinations and the resulting terms for each of those combinations.  
 295 For example, let us assume that there are four independent coagulation events  
 296 within a single timestep: one event between two fresh BC-containing particles  
 297 resulting in an aged particle, two events between fresh and aged BC-containing  
 298 particles each resulting in an aged particle, and one event between a fresh  
 299 BC-containing particle and a non-BC-containing particle resulting in a fresh  
 300 particle. Then we have losses  $\Delta n_{f \rightarrow a}^{\text{coag}}(t_{k-1}, t_k) = 5$  and  $\Delta n_{a \rightarrow a}^{\text{coag}}(t_{k-1}, t_k) = 2$ ,  
 301 and gains  $\Delta n_f^{\text{coag}}(t_{k-1}, t_k) = 1$  and  $\Delta n_a^{\text{coag}}(t_{k-1}, t_k) = 3$ .

302 Note that for each particle pairing in Table 3 there can be two outcomes. For  
 303 example, coagulation of a small fresh and large aged particle generally pro-  
 304 duces an aged particle, while coagulation of large fresh and small aged gener-  
 305 ally produces a fresh particle. When  $S_c$ , as calculated in equations (2)–(3), is  
 306 used as the criterion for fresh versus aged, it can be shown that coagulation  
 307 of two aged particles never produces a fresh particle, and that the coagulation  
 308 of two fresh particles with  $S_c$  values close to the cutoff value can produce an  
 309 aged particle.

Coagulation can result in a net loss of number but must conserve mass. We thus have

$$\dot{N}_a^{\text{coag}}(t) \leq \dot{N}_{f \rightarrow a}^{\text{coag}}(t) + \dot{N}_{a \rightarrow a}^{\text{coag}}(t) \quad (5)$$

$$\dot{M}_a^{\text{coag}}(t) = \dot{M}_{f \rightarrow a}^{\text{coag}}(t) + \dot{M}_{a \rightarrow a}^{\text{coag}}(t) \quad (6)$$

$$\Delta n_a^{\text{coag}}(t_{k-1}, t_k) \leq \Delta n_{f \rightarrow a}^{\text{coag}}(t_{k-1}, t_k) + \Delta n_{a \rightarrow a}^{\text{coag}}(t_{k-1}, t_k) \quad (7)$$

$$\Delta m_a^{\text{coag}}(t_{k-1}, t_k) = \Delta m_{f \rightarrow a}^{\text{coag}}(t_{k-1}, t_k) + \Delta m_{a \rightarrow a}^{\text{coag}}(t_{k-1}, t_k) \quad (8)$$

310 and similarly for coagulation resulting in fresh particles.

The following continuous equations describe the evolution of the number and

mass concentrations of fresh and aged BC-containing populations:

$$\begin{aligned} \frac{dN_f(t)}{dt} = & \dot{N}_f^{\text{density}}(t) + \dot{N}_f^{\text{emit}}(t) - \dot{N}_f^{\text{dilution}}(t) \\ & + \dot{N}_{a \rightarrow f}^{\text{cond}}(t) + \dot{N}_f^{\text{coag}}(t) - \dot{N}_{f \rightarrow f}^{\text{coag}}(t) - \underbrace{\left( \dot{N}_{f \rightarrow a}^{\text{cond}}(t) + \dot{N}_{f \rightarrow a}^{\text{coag}}(t) \right)}_{\dot{N}^{\text{aging}}(t)} \end{aligned} \quad (9)$$

$$\begin{aligned} \frac{dN_a(t)}{dt} = & \dot{N}_a^{\text{density}}(t) + \dot{N}_a^{\text{emit}}(t) - \dot{N}_a^{\text{dilution}}(t) \\ & + \dot{N}_{f \rightarrow a}^{\text{cond}}(t) + \dot{N}_a^{\text{coag}}(t) - \dot{N}_{a \rightarrow a}^{\text{coag}}(t) - \underbrace{\left( \dot{N}_{a \rightarrow f}^{\text{cond}}(t) + \dot{N}_{a \rightarrow f}^{\text{coag}}(t) \right)}_{\dot{N}^{\text{de-aging}}(t)} \end{aligned} \quad (10)$$

$$\begin{aligned} \frac{dM_f(t)}{dt} = & \dot{M}_f^{\text{density}}(t) + \dot{M}_f^{\text{emit}}(t) - \dot{M}_f^{\text{dilution}}(t) \\ & + \underbrace{\left( \dot{M}_{a \rightarrow f}^{\text{cond}}(t) + \dot{M}_{a \rightarrow f}^{\text{coag}}(t) \right)}_{\dot{M}^{\text{de-aging}}(t)} - \underbrace{\left( \dot{M}_{f \rightarrow a}^{\text{cond}}(t) + \dot{M}_{f \rightarrow a}^{\text{coag}}(t) \right)}_{\dot{M}^{\text{aging}}(t)} \end{aligned} \quad (11)$$

$$\begin{aligned} \frac{dM_a(t)}{dt} = & \dot{M}_a^{\text{density}}(t) + \dot{M}_a^{\text{emit}}(t) - \dot{M}_a^{\text{dilution}}(t) \\ & + \underbrace{\left( \dot{M}_{f \rightarrow a}^{\text{cond}}(t) + \dot{M}_{f \rightarrow a}^{\text{coag}}(t) \right)}_{\dot{M}^{\text{aging}}(t)} - \underbrace{\left( \dot{M}_{a \rightarrow f}^{\text{cond}}(t) + \dot{M}_{a \rightarrow f}^{\text{coag}}(t) \right)}_{\dot{M}^{\text{de-aging}}(t)} \end{aligned} \quad (12)$$

311 Note that the mass equations (11)–(12) have been simplified from forms identi-  
 312 cal to the number equations (9)–(10) by using equation (6) for the conservation  
 313 of mass during coagulation. Condensation (or rather evaporation) and coag-  
 314 ulation can in principle also produce a transfer from aged to fresh particles.  
 315 This is reflected by the terms denoted as  $\dot{N}^{\text{de-aging}}(t)$  and  $\dot{M}^{\text{de-aging}}(t)$  above.

The aging time-scales  $\tau_N$  and  $\tau_M$  for number and mass are then determined by the first-order models:

$$\dot{N}^{\text{aging}}(t) = \frac{1}{\tau_N(t)} N_f(t) \quad (13)$$

$$\dot{M}^{\text{aging}}(t) = \frac{1}{\tau_M(t)} M_f(t) \quad (14)$$

The discrete versions of the balance equations (9)–(12) are:

$$\begin{aligned} n_f(t_k) - n_f(t_{k-1}) = & \Delta n_f^{\text{emit}}(t_{k-1}, t_k) - \Delta n_f^{\text{dilution}}(t_{k-1}, t_k) \\ & + \Delta n_{a \rightarrow f}^{\text{cond}}(t_{k-1}, t_k) + \Delta n_f^{\text{coag}}(t_{k-1}, t_k) - \Delta n_{f \rightarrow f}^{\text{coag}}(t_{k-1}, t_k) \\ & - \underbrace{\left( \Delta n_{f \rightarrow a}^{\text{cond}}(t_{k-1}, t_k) + \Delta n_{f \rightarrow a}^{\text{coag}}(t_{k-1}, t_k) \right)}_{\Delta n^{\text{aging}}(t_{k-1}, t_k)} \end{aligned} \quad (15)$$

$$\begin{aligned}
n_a(t_k) - n_a(t_{k-1}) &= \Delta n_a^{\text{emit}}(t_{k-1}, t_k) - \Delta n_a^{\text{dilution}}(t_{k-1}, t_k) \\
&+ \Delta n_{f \rightarrow a}^{\text{cond}}(t_{k-1}, t_k) + \Delta n_a^{\text{coag}}(t_{k-1}, t_k) - \Delta n_{a \rightarrow a}^{\text{coag}}(t_{k-1}, t_k) \\
&- \underbrace{\left( \Delta n_{a \rightarrow f}^{\text{cond}}(t_{k-1}, t_k) + \Delta n_{a \rightarrow f}^{\text{coag}}(t_{k-1}, t_k) \right)}_{\Delta n^{\text{de-aging}}(t_{k-1}, t_k)}
\end{aligned} \tag{16}$$

$$\begin{aligned}
m_f(t_k) - m_f(t_{k-1}) &= \Delta m_f^{\text{emit}}(t_{k-1}, t_k) - \Delta m_f^{\text{dilution}}(t_{k-1}, t_k) \\
&+ \underbrace{\left( \Delta m_{a \rightarrow f}^{\text{cond}}(t_{k-1}, t_k) + \Delta m_{a \rightarrow f}^{\text{coag}}(t_{k-1}, t_k) \right)}_{\Delta m^{\text{de-aging}}(t_{k-1}, t_k)} \\
&- \underbrace{\left( \Delta m_{f \rightarrow a}^{\text{cond}}(t_{k-1}, t_k) + \Delta m_{f \rightarrow a}^{\text{coag}}(t_{k-1}, t_k) \right)}_{\Delta m^{\text{aging}}(t_{k-1}, t_k)}
\end{aligned} \tag{17}$$

$$\begin{aligned}
m_a(t_k) - m_a(t_{k-1}) &= \Delta m_a^{\text{emit}}(t_{k-1}, t_k) - \Delta m_a^{\text{dilution}}(t_{k-1}, t_k) \\
&+ \underbrace{\left( \Delta m_{f \rightarrow a}^{\text{cond}}(t_{k-1}, t_k) + \Delta m_{f \rightarrow a}^{\text{coag}}(t_{k-1}, t_k) \right)}_{\Delta m^{\text{aging}}(t_{k-1}, t_k)} \\
&- \underbrace{\left( \Delta m_{a \rightarrow f}^{\text{cond}}(t_{k-1}, t_k) + \Delta m_{a \rightarrow f}^{\text{coag}}(t_{k-1}, t_k) \right)}_{\Delta m^{\text{de-aging}}(t_{k-1}, t_k)}
\end{aligned} \tag{18}$$

316 Here equation (8) for the discrete conservation of mass during coagulation was  
317 used to simplify the mass equations, as in the continuous case.

By comparing the continuous equations (9)–(12) to the discrete equations (15)–(18) using the relationships (4) we see that the continuous aging terms can be approximated by:

$$\dot{N}^{\text{aging}}(t_k) \approx \frac{\Delta n^{\text{aging}}(t_{k-1}, t_k)}{(t_k - t_{k-1})V(t_k)} \tag{19}$$

$$\dot{M}^{\text{aging}}(t_k) \approx \frac{\Delta m^{\text{aging}}(t_{k-1}, t_k)}{(t_k - t_{k-1})V(t_k)}, \tag{20}$$

318 where the use of  $V$  at time  $t_k$  is because the computational volume  $V$  is  
319 updated first within each timestep in the PartMC algorithm (Riemer et al.,  
320 2009, Figure 1).

From equations (13) and (14) and the relationships (4), the aging time-scales  $\tau_N$  and  $\tau_M$  are then approximated by:

$$\tau_N(t_k) \approx \frac{(t_k - t_{k-1})n_f(t_k)}{\Delta n^{\text{aging}}(t_{k-1}, t_k)} \tag{21}$$

$$\tau_M(t_k) \approx \frac{(t_k - t_{k-1})m_f(t_k)}{\Delta m^{\text{aging}}(t_{k-1}, t_k)}. \tag{22}$$

For the analysis in Section 5 we additionally define the aging time-scale  $\tau_N^{\text{cond}}$  ignoring the impact of coagulation, an average time-scale  $\tau_{N,\text{day}}$  during the day, and an average time-scale  $\tau_{N,\text{night}}$  during the night, given by:

$$\tau_N^{\text{cond}}(t_k) \approx \frac{(t_k - t_{k-1})n_f(t_k)}{\Delta n_{f \rightarrow a}^{\text{cond}}(t_{k-1}, t_k)} \quad (23)$$

$$(\tau_{N,\text{day}})^{-1} = \frac{1}{3 \text{ hours}} \int_{12:00 \text{ LST}}^{15:00 \text{ LST}} (\tau_N(t))^{-1} dt \quad (24)$$

$$(\tau_{N,\text{night}})^{-1} = \frac{1}{10 \text{ hours}} \int_{18:00 \text{ LST}}^{04:00 \text{ LST}} (\tau_N(t))^{-1} dt, \quad (25)$$

and similarly for  $\tau_M^{\text{cond}}$ ,  $\tau_{M,\text{day}}$ ,  $\tau_{M,\text{night}}$ ,  $\tau_{N,\text{day}}^{\text{cond}}$ , and so on.

## 5 Results

In this section we show results for supersaturation thresholds ranging between  $S_c = 0.1\%$  and  $S_c = 1.0\%$ , as these are typically achieved in updrafts in stratus and cumulus clouds (Warner, 1968). To limit the number of figures we use  $S_c = 0.6\%$  as a base case. Figure 5 shows the time series for  $N_f$ ,  $N_a$ , and  $N_{\text{BC}} = N_f + N_a$  for  $S_c = 0.6\%$ . The total number concentration  $N_{\text{BC}}$  of BC-containing particles increased until 18:00 LST due to the emission of particles. After the emissions stopped,  $N_{\text{BC}}$  decreased as a result of continued dilution and coagulation. The time series for  $N_f$  and  $N_a$  show that both increased in the morning hours. A pronounced transfer from fresh to aged occurred after 11:30 LST, the time when nitrate formation started taking place on the dry particles (compare Figure 2). This process efficiently contributed to the conversion of fresh particles to aged particles, which was reflected by a short aging time-scale.

The left column of Figure 6 compares the aging time-scales  $\tau_N$  and  $\tau_N^{\text{cond}}$  computed according to equations (21) and (23) for different supersaturation thresholds. The top, middle and bottom panels shows the results for supersaturation thresholds  $S_c = 0.1\%$ ,  $S_c = 0.6\%$ , and  $S_c = 1\%$ , respectively. The grey shading is the raw data, and the black lines are results computed from smoothing the transfer rates with a Hann filter with a window width of 1 hour.

The solid lines represent  $\tau_N$ , including the contributions due to both coagulation and condensation according to equation (21). For  $S_c = 0.6\%$ ,  $\tau_N$  started off in the morning with values of  $\tau_N \approx 20$  hours. It decreased sharply after 11:00 LST, which is the time when photochemistry was at its peak, and nitrate formation was most pronounced, hence leading to a fast aging process. Between 12:00 LST and 16:00 LST,  $\tau_N$  was less than 1 hour, and reached values as low as 0.2 hours. After 16:00 LST, as photochemistry slowed down,  $\tau_N$

increased again, reaching a plateau of  $\tau_N \approx 10$  hours during the evening and night.

The broken lines represent  $\tau_N^{\text{cond}}$  as defined in equation (23), i.e. the contribution due to coagulation is ignored. There was only a small difference between  $\tau_N$  and  $\tau_N^{\text{cond}}$  during midday and early afternoon when condensation was operating very effectively. However during morning, afternoon and night, neglecting coagulation lead to larger time-scales (up to one order of magnitude).

A similar pattern was found for  $S_c = 1\%$ , shown in the bottom panel. For  $S_c = 0.1\%$  we generally obtained larger time-scales. During the morning,  $\tau_N$  was about 50 hours and decreased to 10 hours in the early afternoon. There was a short period around 16:00 LST when  $\tau_N$  dropped to 2 hours. Obviously, at  $S_c = 0.1\%$ , even after the growth due to condensation of ammonium nitrate, the particles were still too small to be activated to the same extent as seen for the larger supersaturations. During the following night  $\tau_N$  was around 10–20 hours. For this low supersaturation the contrast between day and night was not as pronounced as for  $S_c = 0.6\%$  or  $S_c = 1\%$ .

Qualitatively, the temporal evolution of  $\tau_M$  (right column) was similar to the number-based result  $\tau_N$ . However the day/night contrast was more pronounced for the case with  $S_c = 0.1\%$ , and the time-scales based on mass during the day were lower than the ones based on number.

Figure 7 shows the individual transfer terms of BC-containing particles for the case  $S_c = 0.6\%$ . The transfer rate  $\dot{N}_{a \rightarrow f}^{\text{coag}}$  due to coagulation from aged to fresh was very small throughout the whole day, remaining below  $0.01 \text{ cm}^{-3} \text{ s}^{-1}$ . The transfer rate  $\dot{N}_{f \rightarrow a}^{\text{coag}}$  due to coagulation from fresh to aged followed the time series of  $N_f$ . The minimum of  $N_f$  during the early afternoon was reflected in a minimum of the transfer rate  $\dot{N}_{f \rightarrow a}^{\text{coag}}$ . The transfer rate  $\dot{N}_{f \rightarrow a}^{\text{cond}}$  due to condensation from fresh to aged was large between 11:30 and 15:00 LST, consistent with the decrease of  $\tau_N$  in Figure 6. Lastly, there was a non-zero transfer  $\dot{N}_{a \rightarrow f}^{\text{cond}}$  from aged to fresh due to condensation, which was larger than  $\dot{N}_{f \rightarrow a}^{\text{cond}}$  towards the end of the simulation. This was related to a shrinking of the particles due to decreasing relative humidity (compare Figure 1).

Figure 8 summarizes the results for the different aging time-scale definitions. We calculated  $\tau_{N,\text{day}}$  and  $\tau_{N,\text{night}}$  according to equation (23) for several hundred different supersaturation thresholds between  $S_c = 0.1\%$  and  $S_c = 1\%$ . We also distinguished between the definition of  $\tau$  including the transfer due to coagulation and condensation (solid lines), and including only the transfer due to condensation,  $\tau_{N,\text{day}}^{\text{cond}}$  and  $\tau_{N,\text{night}}^{\text{cond}}$  (broken lines).

For this particular urban plume scenario the following general features emerge: during the day, condensation of semi-volatile species, in our case especially ammonium nitrate, was the dominant process for aging. The time-scales based

on number were larger than the time-scales based on mass during the day, by roughly a factor of five. The aging time-scales had a strong dependence on supersaturation threshold. For  $S_c = 0.1\%$ ,  $\tau_{N,\text{day}}$  was 10 hours, whereas for  $S_c = 1\%$ ,  $\tau_{N,\text{day}}$  was only 0.2 hours. During the night condensation was limited, hence coagulation was the dominant aging process. For low supersaturation thresholds, the time-scales based on number were smaller than the time-scales based on mass, but this difference decreased for higher supersaturation thresholds.

## 6 Conclusions

In this paper we presented a method for explicitly calculating aging time-scales of black carbon aerosol using particle-resolved model simulations with PartMC-MOSAIC. We developed number-based and mass-based aging time-scales using the activation of the particles at a given supersaturation as a criterion for aging. We applied this method to an urban plume scenario (Riemer et al., 2009) for a range of supersaturation thresholds between 0.1% and 1% and considered condensation of secondary substances and coagulation as aging mechanisms. Aging due to heterogeneous processes (chemical aging) were not included.

For this particular scenario we found a separation into day and night regimes. During the day the condensation-induced aging dominated, in particular due to the formation of ammonium nitrate. Therefore the condensation-only number-based aging time-scale  $\tau_{N,\text{day}}^{\text{cond}}$  was almost the same as the total time-scale  $\tau_{N,\text{day}}$  and similarly for mass. The daytime aging number-based time-scale  $\tau_{N,\text{day}}$  was about 10 hours for a supersaturation threshold of  $S_c = 0.1\%$  and decreased to 0.06 hours for a threshold of  $S_c = 1\%$ . The daytime mass-based aging time-scale  $\tau_{M,\text{day}}$  was about a factor of five lower than  $\tau_{N,\text{day}}$  for all supersaturation thresholds.

During the night, the absence of condensable species caused the number-based aging time-scale  $\tau_{N,\text{night}}$  to be about one order of magnitude larger than during the day. Coagulation became dominant, which was reflected by the fact that the condensation-only time-scale  $\tau_{N,\text{night}}^{\text{cond}}$  was an order of magnitude larger than the total time-scale  $\tau_{N,\text{night}}$ . The nighttime aging time-scales therefore depended on the particle number concentrations. We suspect that chemical aging would have its largest impact during periods when condensation is not dominant, i.e. during the night in our case.

Compared to the time-scales used in global models, which are typically on the order of 30 hours (Chung and Seinfeld, 2002; Koch, 2001, e.g.), our time-scales were much shorter, in particular during the day. This confirmed findings by

427 Riemer et al. (2004) who showed with a completely different approach that  
428 daytime and nighttime aging regimes exists, and that aging during the day  
429 proceeds very rapidly.

430 However some caveats need to be emphasized: our urban plume scenario repre-  
431 sents only one scenario, with very polluted conditions and fairly high number  
432 concentrations during the night ( $N_{\text{BC}} \approx 5000 \text{ cm}^{-3}$ ). For lower number con-  
433 centrations, we expect the aging time-scales during the night to increase.

434 **Acknowledgments.** Funding for N. Riemer and M. West was provided by  
435 the National Science Foundation (NSF) under grant ATM 0739404. Funding  
436 for R. A. Zaveri and R. C. Easter was provided by the Aerosol-Climate Initia-  
437 tive as part of the Pacific Northwest National Laboratory (PNNL) Laboratory  
438 Directed Research and Development (LDRD) program. Pacific Northwest Na-  
439 tional Laboratory is operated for the U.S. Department of Energy by Battelle  
440 Memorial Institute under contract DE-AC06-76RLO 1830.

## 441 References

- 442 Andreae, M., Gelenc  ser, A., 2006. Black carbon or brown carbon? The nature  
443 of light-absorbing carbonaceous aerosols. *Atmos. Chem. Phys.* 6, 3131–3148.
- 444 Bond, T., Streets, D., Yarber, K., Nelson, S., Woo, J., Klimont, Z., 2004. A  
445 technology-based global inventory of black and organic carbon emissions  
446 from combustion. *J. Geophys. Res* 109 (D14), D14203.
- 447 Chung, S. H., Seinfeld, J. H., 2002. Global distribution and climate forcing of  
448 carbonaceous aerosols. *J. Geophys. Res.* 107.
- 449 Clegg, S., Brimblecombe, P., Wexler, A., 1998. Thermodynamic model of the  
450 system  $\text{H}^+ - \text{NH}_4^+ - \text{Na}^+ - \text{SO}_4^{2-} - \text{NH}_3 - \text{Cl}^- - \text{H}_2\text{O}$  at 298.15 K. *J. Phys. Chem. A*  
451 102 (12), 2155–2171.
- 452 Cooke, W. F., Lioussse, C., Cachier, H., Feichter, J., 1999. Construction of a  
453  $1^\circ \times 1^\circ$  fossil fuel emission data set for carbonaceous aerosol and implemen-  
454 tation and radiative impact in the ECHAM4 model. *J. Geophys. Res.* 104,  
455 22137–22162.
- 456 Croft, B., Lohmann, U., von Salzen, K., 2005. Black carbon aging in the  
457 Canadian Centre for Climate modelling and analysis atmospheric gener-  
458 al circulation model. *Atmos. Chem. Phys.* 5, 1931–1949, sRef-ID:1680-  
459 7324/acp/2005-5-1931.
- 460 Cubison, M. J., Ervens, B., Feingold, G., Docherty, K. S., Ulbrich, I. M.,  
461 Shields, L., Prather, K., Hering, S., Jimenez, J. L., 2008. The influence of  
462 chemical composition and mixing state on Los Angeles urban aerosol on  
463 CCN number and cloud properties. *Atmos. Chem. Phys. Discuss.* 8, 5629–  
464 5681.

- 465 Eldering, A., Cass, G. R., 1996. Source-oriented model for air pollution effects  
466 on visibility. *J. Geophys. Res.* 101, 19343–19369.
- 467 Furutani, H., Dallosto, M., Roberts, G., Prather, K., 2008. Assessment of the  
468 relative importance of atmospheric aging on CCN activity derived from field  
469 observations. *Atmos. Environ.* 42 (13), 3130–3142.
- 470 Ghan, S., Laulainen, N., Easter, R., Wagener, R., Nemesure, S., Chapman, E.,  
471 Zhang, Y., Leung, R., 2001. Evaluation of aerosol direct radiative forcing in  
472 MIRAGE. *Journal of Geophysical Research* 106 (D6), 5317–5334.
- 473 Horvath, H., Trier, A., 1993. A study of the aerosol of Santiago de Chile — I.  
474 Light extinction coefficient. *Atmos. Environ.* 27, 371–384.
- 475 IPCC, 2007. Climate Change 2007: The physical science basis summary for  
476 policymakers. Contribution of working group I to the fourth assessment re-  
477 port of the Intergovernmental Panel on Climate Change. World Meteorolo-  
478 gical Organization, Geneva, Switzerland.
- 479 Jaenicke, R., 1993. Aerosol-Cloud-Climate Interaction. Academic Press, San  
480 Diego, CA, Ch. Tropospheric aerosols, pp. 1–31.
- 481 Kittelson, D., Watts, W., Johnson, J., 2006a. On-road and laboratory evalu-  
482 ation of combustion aerosols — Part 1: Summary of diesel engine results.  
483 *Aerosol Sci.* 37, 913–930.
- 484 Kittelson, D., Watts, W., Johnson, J., Schauer, J., Lawson, D., 2006b. On-  
485 road and laboratory evaluation of combustion aerosols — Part 2: Summary  
486 of spark ignition engine results. *Aerosol Sci.* 37, 931–949.
- 487 Kleeman, M., Schauer, J., Cass, G., 2000. Size and composition distribution of  
488 fine particulate matter emitted from motor vehicles. *Environ. Sci. Technol.*  
489 34, 1132–1142.
- 490 Koch, D., 2001. Transport and direct radiative forcing of carbonaceous and  
491 sulfate aerosols in the GISS GCM. *J. Geophys. Res.* 106, 20311–20332.
- 492 Lohmann, U., Feichter, J., Chuang, C. C., Penner, J. E., 1999. Prediction of  
493 the number of cloud droplets in the ECHAM GCM. *J. Geophys. Res.* 104,  
494 9169–9198.
- 495 McFiggans, G., Artaxo, P., Baltensperger, U., Coe, H., Facchini, M. C., Fein-  
496 gold, G., Fuzzi, S., Gysel, M., Laaksonen, A., Lohmann, U., Mentel, T. F.,  
497 Murphy, D. M., O’Dowd, C. D., Snider, J. R., Weingartner, E., 2006. The  
498 effect of physical and chemical aerosol properties on warm cloud droplet  
499 activation. *Atmos. Chem. Phys.* 6, 2593–2649.
- 500 McMurry, P., Stolzenburg, M., 1989. On the sensitivity of particle size to  
501 relative humidity for Los Angeles aerosols. *Atmospheric Environment* (1967)  
502 23 (2), 497–507.
- 503 Medalia, A., Rivin, D., 1982. Particulate carbon and other components of soot  
504 and carbon black. *Carbon* 20, 481–492.
- 505 Menon, S., Hansen, J., Nazarenko, L., Luo, Y. F., 2002. Climate effects of  
506 black carbon aerosols in China and India. *Science* 297, 2250–2253.
- 507 Moffet, R., Qin, X., Rebotier, T., Furutani, H., Prather, K., 2008. Chemically  
508 segregated optical and microphysical properties of ambient aerosols mea-  
509 sured in a single-particle mass spectrometer. *J. Geophys. Res.* 113 (D12),

510 D12213.

511 Petters, M., Prenni, A., Kreidenweis, S., DeMott, P., Matsunaga, A., Lim,  
512 Y., Ziemann, P., 2006. Chemical aging and the hydrophobic-to-hydrophilic  
513 conversion of carbonaceous aerosol. *Geophys. Res. Lett* 33, L24806.

514 Petters, M. D., Kreidenweis, S. M., 2007. A single parameter representation of  
515 hygroscopic growth and cloud condensation nucleus activity. *Atmos. Chem.*  
516 *Phys.* 7, 1961–1971.

517 Pöschl, U., 2005. Atmospheric aerosols: Composition, transformation, climate  
518 and health effects. *Angew. Chem. Int. Ed. Engl.* 44, 752–754.

519 Prenni, A., Petters, M., Kreidenweis, S., DeMott, P., Ziemann, P., 2007.  
520 Cloud droplet activation of secondary organic aerosol. *J. Geophys. Res* 112,  
521 D10223.

522 Press, W. H., Teukolsky, S. A., Vetterling, W. T., Flannery, B. P., 2007. Nu-  
523 merical Recipes: The Art of Scientific Computing, 3rd Edition. Cambridge  
524 University Press.

525 Riemer, N., Vogel, H., Vogel, B., 2004. Soot aging time scales in polluted  
526 regions during day and night. *Atmospheric Chemistry and Physics* 4, 1885–  
527 1893.

528 Riemer, N., Vogel, H., Vogel, B., Fiedler, F., 2003. Modeling aerosols on the  
529 mesoscale  $\gamma$ , part I: Treatment of soot aerosol and its radiative effects. *J.*  
530 *Geophys. Res.* 108, 4601.

531 Riemer, N., West, M., Zaveri, R., Easter, R., 2009. Simulating the evolution of  
532 soot mixing state with a particle-resolved aerosol model. *J. Geophys. Res.*In  
533 press.

534 Rudich, Y., Donahue, N. M., Mentel, T. F., 2007. Aging of organic aerosol:  
535 Bridging the gap between laboratory and field studies. *Annual Rev. Phys.*  
536 *Chem.* 58, 321–352.

537 Schell, B., Ackermann, I. J., Binkowski, F. S., Ebel, A., 2001. Modeling the  
538 formation of secondary organic aerosol within a comprehensive air quality  
539 model system. *J. Geophys. Res.* 106, 28275–28293.

540 Svenningsson, B., Rissler, J., Swietlicki, E., Mircea, M., Bilde, M., Facchini,  
541 M., Decesari, S., Fuzzi, S., Zhou, J., Mønster, J., et al., 2006. Hygroscopic  
542 growth and critical supersaturations for mixed aerosol particles of inorganic  
543 and organic compounds of atmospheric relevance. *Atmos. Chem. Phys* 6,  
544 1937–1952.

545 Toner, S., Sodeman, S., Prather, K., 2006. Single particle characterization of  
546 ultrafine and accumulation mode particles from heavy duty diesel vehicles  
547 using aerosol time-of-flight mass spectrometry. *Environ. Sci. Technol.* 40,  
548 3912–3921.

549 Warner, J., 1968. The supersaturation in natural clouds. *J. Appl. Meteorol.*  
550 7, 233–237.

551 Weingartner, E., Burtscher, H., Baltensperger, H., 1997. Hygroscopic proper-  
552 ties of carbon and diesel soot particles. *Atmos. Environ.* 31, 2311–2327.

553 Zaveri, R. A., Easter, R. C., Fast, J. D., Peters, L. K., 2008. Model for Sim-  
554 ulating Aerosol Interactions and Chemistry (MOSAIC). *J. Geophys. Res.*

113, D13204.  
Zaveri, R. A., Easter, R. C., Peters, L. K., 2005a. A computationally efficient  
Multicomponent Equilibrium Solver for Aerosols (MESA). J. Geophys. Res.  
110, D24203.  
Zaveri, R. A., Easter, R. C., Wexler, A. S., 2005b. A new method for multicom-  
ponent activity coefficients of electrolytes in aqueous atmospheric aerosols.  
J. Geophys. Res. 110, D02210, doi:10.1029/2004JD004681.  
Zaveri, R. A., Peters, L. K., 1999. A new lumped structure photochemical  
mechanism for large-scale applications. J. Geophys. Res. 104, 30387–30415.

Initial/Background	$N$ ( $\text{m}^{-3}$ )	$D_{\text{gn}}$ ( $\mu\text{m}$ )	$\sigma_{\text{g}}$ (1)	Composition by mass
Aitken Mode	$3.2 \cdot 10^9$	0.02	1.45	50% $(\text{NH}_4)_2\text{SO}_4$ , 50% POA
Accumulation Mode	$2.9 \cdot 10^9$	0.116	1.65	50% $(\text{NH}_4)_2\text{SO}_4$ , 50% POA

Emissions	$E$ ( $\text{m}^{-2} \text{s}^{-1}$ )	$D_{\text{gn}}$ ( $\mu\text{m}$ )	$\sigma_{\text{g}}$ (1)	Composition by mass
Meat cooking	$9 \cdot 10^6$	0.086	1.9	100% POA
Diesel vehicles	$1.6 \cdot 10^8$	0.05	1.7	30% POA, 70% BC
Gasoline vehicles	$5 \cdot 10^7$	0.05	1.7	80% POA, 20% BC

Table 1

Initial and emitted aerosol distribution parameters. The initial aerosol distribution is also used as the background aerosol distribution. The percentages for the composition are by mass.  $E$  is the area source strength of particle emissions. Dividing  $E$  by the mixing height and multiplying by a normalized composition distribution gives the number distribution emission rate.

Terms	Description
$N_f(t), N_a(t)$	Number concentration of fresh/aged BC-containing particles.
$\dot{N}_f^{\text{emit}}(t), \dot{N}_a^{\text{emit}}(t)$	Gain rate of number concentration of fresh/aged BC-containing particles due to emission.
$\dot{N}_f^{\text{dilution}}(t), \dot{N}_a^{\text{dilution}}(t)$	Loss rate of number concentration of fresh/aged BC-containing particles due to dilution.
$\dot{N}_{f \rightarrow a}^{\text{cond}}(t), \dot{N}_{a \rightarrow f}^{\text{cond}}(t)$	Gain rate of number concentration of aged/fresh BC-containing particles due to condensation or evaporation on fresh/aged particles.
$\dot{N}_f^{\text{coag}}(t), \dot{N}_a^{\text{coag}}(t)$	Gain rate of number concentration of fresh/aged BC-containing particles from coagulation events.
$\dot{N}_{f \rightarrow f}^{\text{coag}}(t), \dot{N}_{f \rightarrow a}^{\text{coag}}(t)$	Loss rate of number concentration of fresh BC-containing particles to coagulation events resulting in fresh/aged particles.
$\dot{N}_{a \rightarrow a}^{\text{coag}}(t), \dot{N}_{a \rightarrow f}^{\text{coag}}(t)$	Loss rate of number concentration of aged BC-containing particles to coagulation events resulting in aged/fresh particles.
$\dot{N}_f^{\text{density}}(t), \dot{N}_a^{\text{density}}(t)$	Gain rate of number concentration of fresh/aged BC-containing particles due to air density changes.
$\dot{N}^{\text{aging}}(t), \dot{N}^{\text{de-aging}}(t)$	Net transfer rate of fresh-to-aged/aged-to-fresh number concentration of BC-containing particles.

Table 2

Description of individual terms in equations (9) and (10). With the exception of  $\dot{N}_f^{\text{density}}(t)$  and  $\dot{N}_a^{\text{density}}(t)$  all of these terms must be non-negative. The same notation is for the terms in equations (11) and (12) for mass concentration, and for the corresponding discrete equations (15)–(18). The discrete terms are expressed as a change in number or mass within a timestep, so that  $\Delta n_{f \rightarrow a}^{\text{cond}}(t_{k-1}, t_k)$  is the number of BC-containing particles in the computational volume that change from fresh to aged due only to condensation during the timestep from time  $t_{k-1}$  to  $t_k$ , for example. There are no discrete terms for air density changes as they are incorporated by changing the computational volume  $V$ .

Particle 1	Particle 2	Resulting particle	Non-zero loss terms	Non-zero gain terms
fresh	fresh	fresh	$\Delta n_{f \rightarrow f}^{\text{coag}} = 2$	$\Delta n_f^{\text{coag}} = 1$
fresh	fresh	aged	$\Delta n_{f \rightarrow a}^{\text{coag}} = 2$	$\Delta n_a^{\text{coag}} = 1$
aged	fresh	fresh	$\Delta n_{a \rightarrow f}^{\text{coag}} = 1, \Delta n_{f \rightarrow f}^{\text{coag}} = 1$	$\Delta n_f^{\text{coag}} = 1$
aged	fresh	aged	$\Delta n_{a \rightarrow a}^{\text{coag}} = 1, \Delta n_{f \rightarrow a}^{\text{coag}} = 1$	$\Delta n_a^{\text{coag}} = 1$
aged	aged	aged	$\Delta n_{a \rightarrow a}^{\text{coag}} = 2$	$\Delta n_a^{\text{coag}} = 1$
fresh	non-BC	fresh	$\Delta n_{f \rightarrow f}^{\text{coag}} = 1$	$\Delta n_f^{\text{coag}} = 1$
fresh	non-BC	aged	$\Delta n_{f \rightarrow a}^{\text{coag}} = 1$	$\Delta n_a^{\text{coag}} = 1$
aged	non-BC	fresh	$\Delta n_{a \rightarrow f}^{\text{coag}} = 1$	$\Delta n_f^{\text{coag}} = 1$
aged	non-BC	aged	$\Delta n_{a \rightarrow a}^{\text{coag}} = 1$	$\Delta n_a^{\text{coag}} = 1$

Table 3

The different coagulation events and the resulting expressions for the loss and gain terms of the number of fresh and aged BC-containing particles. Similar expressions exist for mass changes  $\Delta m$  in the particle-resolved model and for the number rates  $\dot{N}$  and mass rates  $\dot{M}$  in the continuous model.

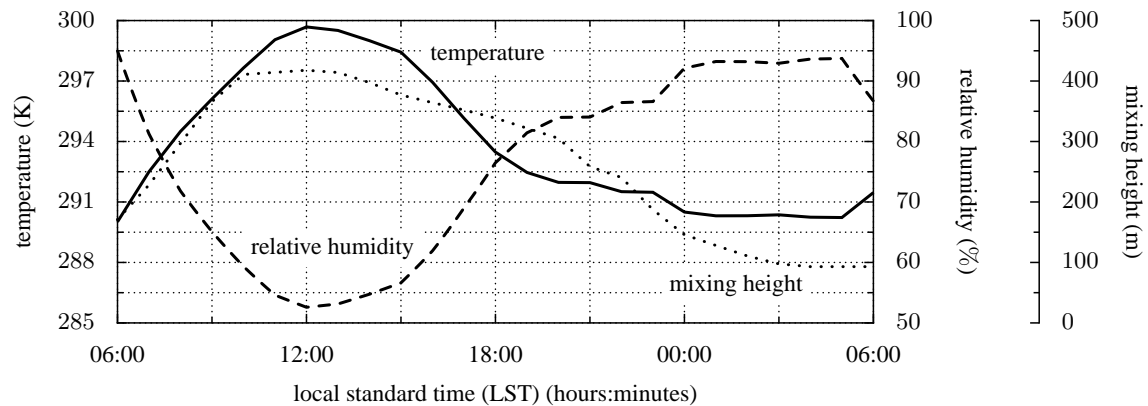


Fig. 1. Time series of temperature, relative humidity, and mixing height over the course of the 24 hour simulation. The pressure and water mixing ratio were kept constant.

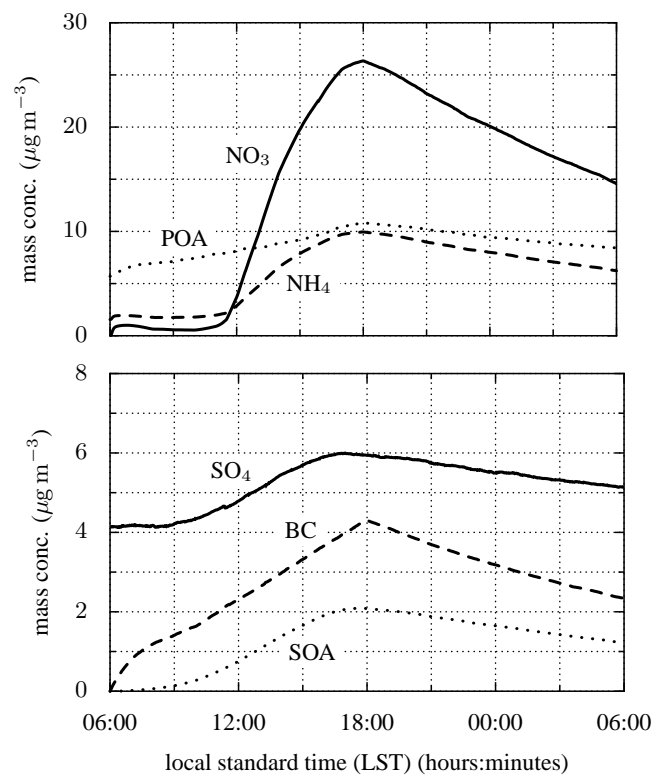


Fig. 2. Time series of mass concentrations of selected aerosol species: nitrate ( $\text{NO}_3$ ), ammonium ( $\text{NH}_4$ ), POA, sulfate ( $\text{SO}_4$ ), BC, and SOA. Particle and gas phase emissions were present from 06:00 to 18:00 LST.

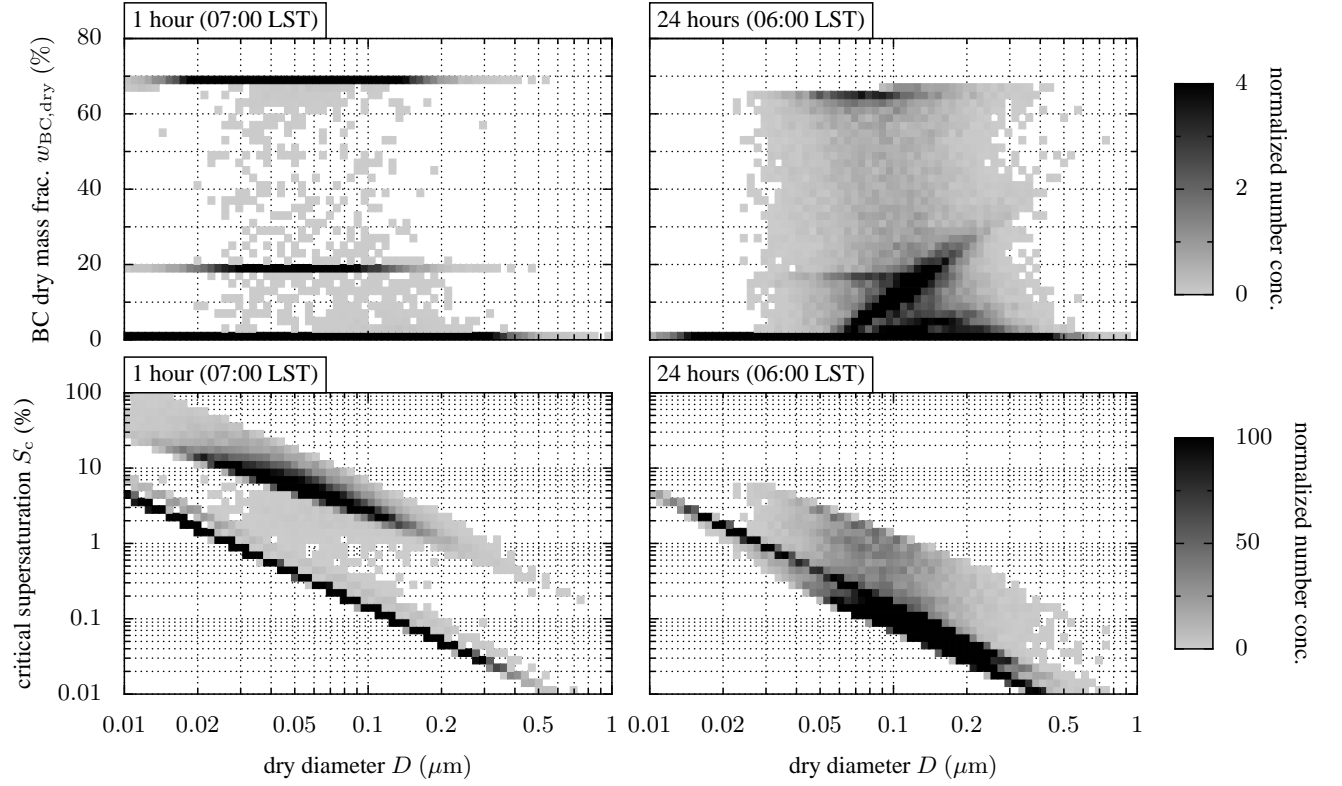


Fig. 3. Normalized two-dimensional number distributions after 1 hour (07:00 LST) and 24 hours (06:00 LST the next day) of simulation. The top panels show the normalized value of the two-dimensional distribution  $\partial^2 N_{\text{BC,dry}}(D, w)/(\partial \log_{10} D \partial w)$  with respect to diameter  $D$  and BC dry mass fraction  $w_{\text{BC,dry}}$ , while the bottom panels show the normalized value of the two-dimensional distribution  $\partial^2 N_{\text{S}}(D, S_c)/(\partial \log_{10} D \partial \log_{10} S_c)$  with respect to diameter  $D$  and critical supersaturation  $S_c$ .

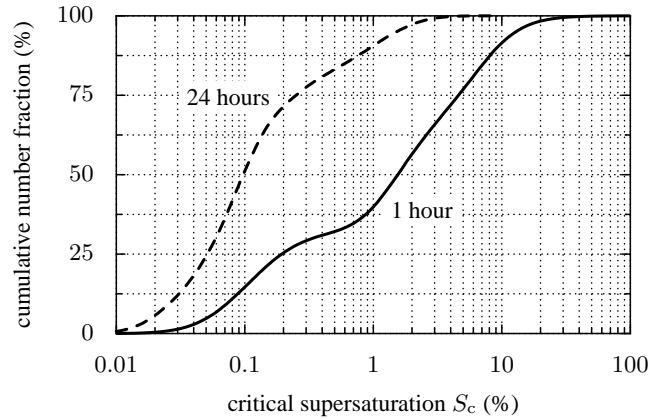


Fig. 4. Cloud condensation nuclei spectra after 1 hour (07:00 LST) and 24 hours (06:00 LST the next day) of simulation based on the simulation results shown in Figure 3.

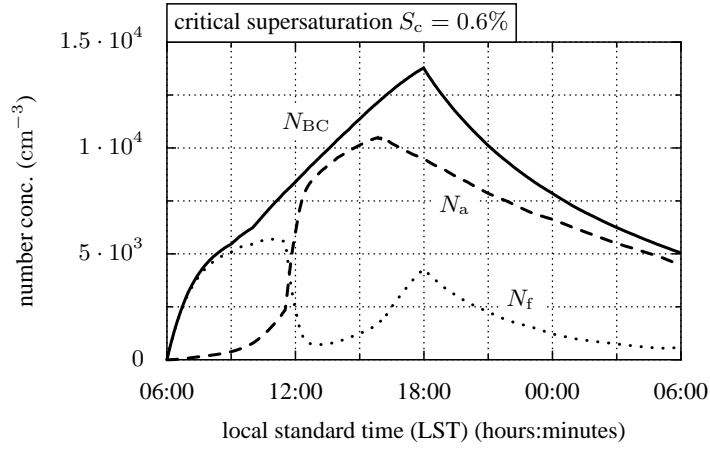


Fig. 5. Time series of total number concentration  $N_{BC}$  of BC-containing particles and number concentrations  $N_f$  and  $N_a$  for fresh and aged BC-containing particles, respectively. The critical supersaturation separating fresh and aged particles is set to  $S_c = 0.6\%$ .

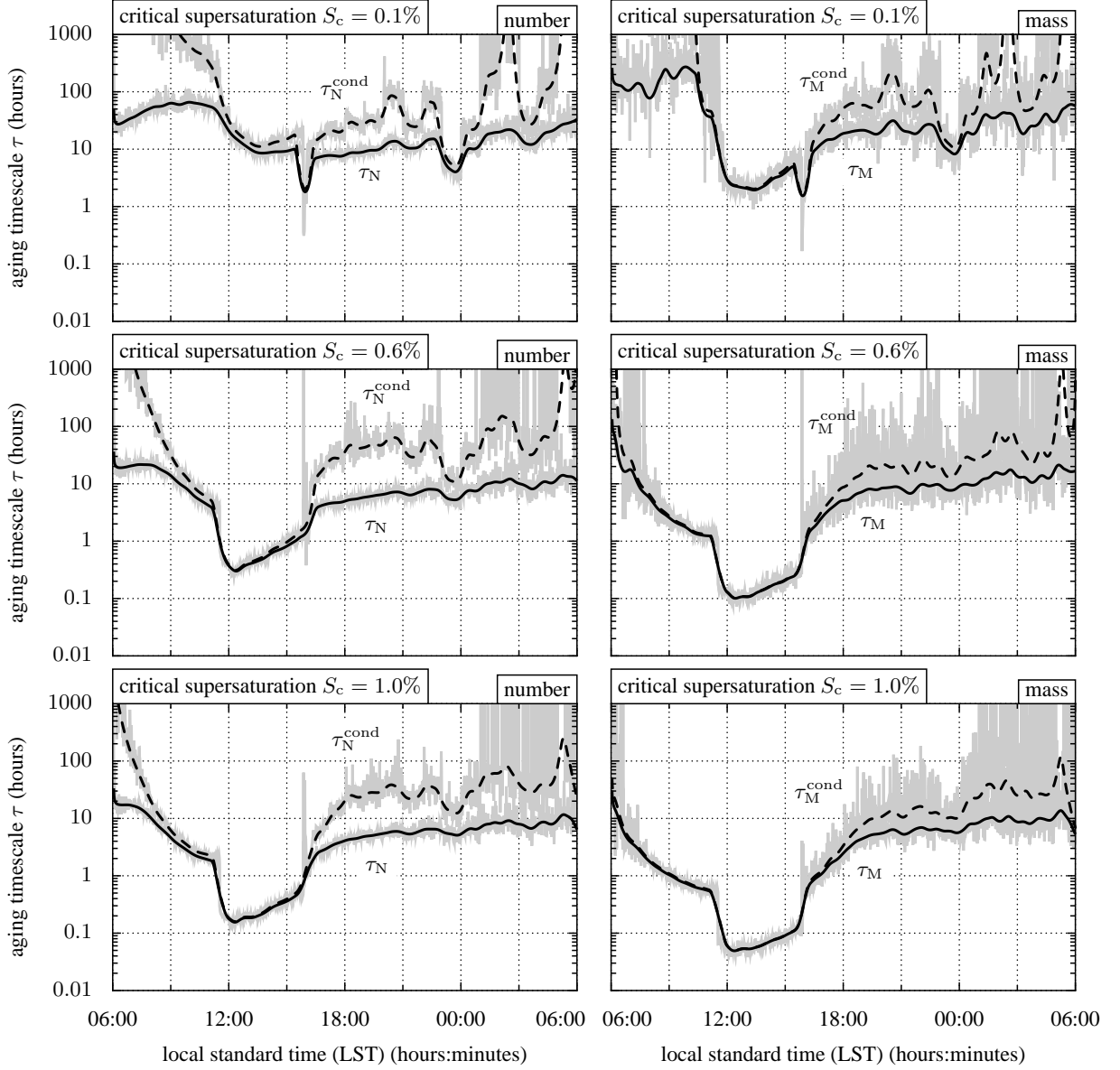


Fig. 6. Comparison of aging time-scales based on number (left) and mass (right), showing both the time-scales due to condensation and coagulation ( $\tau_N$  and  $\tau_M$ ) and the time-scales due to condensation alone ( $\tau_N^{\text{cond}}$  and  $\tau_M^{\text{cond}}$ ). The top panels have the critical supersaturation separating fresh from aged particles set to  $S_c = 0.1\%$ , while the middle panels have  $S_c = 0.6\%$ , and the bottom panels have  $S_c = 1.0\%$ .

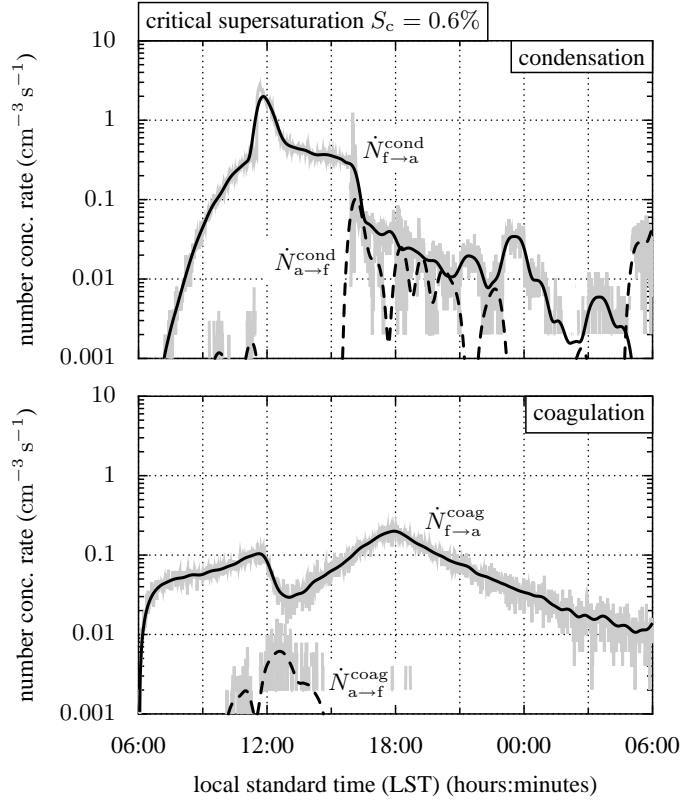


Fig. 7. Transfer rates due to condensation (top) and coagulation (bottom). The critical supersaturation separating fresh and aged particles is set to  $S_c = 0.6\%$ . The notation is according to Table 2.

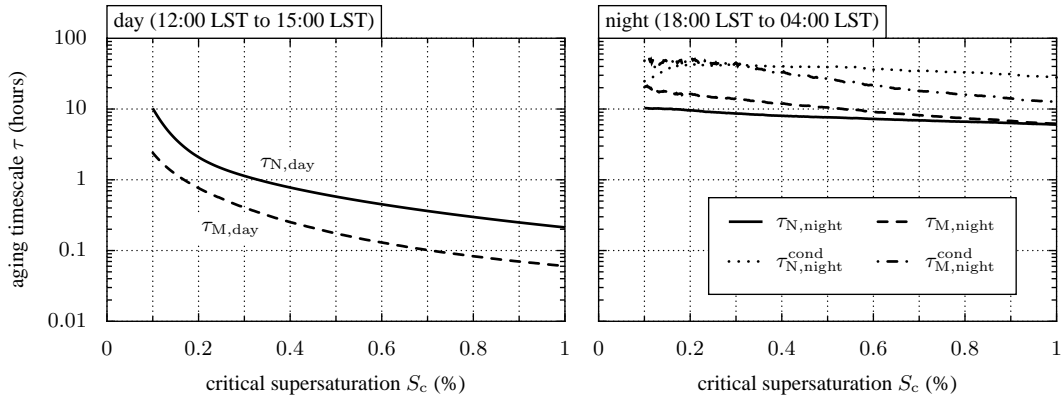


Fig. 8. Day (left) and night (right) averages of the aging time-scale, as defined in equations (23)–(25). As can be seen from Figure 6, during the day the condensation-induced aging dominates, so  $\tau_{N,\text{day}}^{\text{cond}}$  is almost indistinguishable from  $\tau_{N,\text{day}}$ , and similarly for mass.